Fluorescence Switching of Natural Fibers with in-situ Formation of Gold Nanoclusters

Yong Yu,[1]* Ying Chuan Tan,[2] Gorelik Sergey,[3] Yihao Leow,[1] Hui Ru Tan,[1] Chi-Lik Ken Lee [4], Qiang Zhu[1,2,4], Enyi Ye,[1,2,4] Le Yang,[1,5] Dan Kai *[1,2,4]

[1] Institute of Materials Research and Engineering (IMRE), A*STAR, 2 Fusionopolis Way, #08-03, Innovis, 138634, Singapore

[2] Institute of Sustainability for Chemicals, Energy and Environment (ISCE2), A*STAR, 2 Fusionopolis Way, Innovis, #08-03, 138634, Singapore

[3] Singapore Institute of Food and Biotechnology Innovation (SIFBI), A*STAR, 31 Biopolis Way, #01-02, Nanos, 138669, Singapore

[4] Division of Chemistry and Biological Chemistry, School of Physical and Mathematical Sciences, Nanyang Technological University, 21 Nanyang Link, Singapore 637371, Singapore

[5]Department of Materials Science and Engineering, College of Design and Engineering, 9 Engineering Drive 1, National University of Singapore, 117575, Singapore

Email: yuy@imre.a-star.edu.sg; kaid@imre.a-star.edu.sg

Abstract

Natural fibers are a class of thread-like bio-based materials with merits of favorable mechanical properties, low cost, and minimal environmental impact, etc. Endowing additional functionalities to natural fibers would further encourage greater utilization of these renewable materials. In this work, we present a new strategy to integrate ultrasmall (<3 nm) gold nanoclusters (AuNC) with coconut fibers (coir), which resulted in a unique fluorescence switchable composite material. Specifically, we demonstrate that the delignified, green-emissive coir can act as a heterogeneous reducing and nucleating agent to form luminescent AuNC. The immobilization of AuNC switches the intrinsic green emission of delignified coir into enhanced orange emission of the resultant composite material. Our further investigations suggest that the fluorescence switching is governed by the Förster resonance energy transfer (FRET) process despite their disparity in material type, morphology, and size. Several important parameters, such as the FRET efficiency (E), rate constant (k_T), the Förster radius (R_0) and the distance between donor-acceptor pair (R_{DA}) were estimated to describe the FRET process. The distance-sensitive FRET process was also confirmed by varying the medium between the AuNC and delignified coir, which highlighted the potential uses in stimuli-responsive sensor applications. We expect that this strategy can be extended to rationally design functional nature-based materials from various sources.

Keywords: Nanoclusters, Lignocellulosic biomass, Cellulose, Photoswitch, Fluorescence resonance energy transfer, Hybrid organic-inorganic material

1. Introduction

Natural fibers are a class of thread-like materials that are sourced from plants or animals, such as cotton, coconut fibers (coir), bamboo, silk, etc. They are attractive for their sustainability, low cost, low specific weight with high specific strength and stiffness, good thermal and acoustic isolation properties, and therefore have found wide applications, including construction, textile, decoration, storage and packaging(Silva, *et al.*, 2020, Hasan, *et al.*, 2021, Berardi and Iannace, 2015). Despite their many merits, materials scientists are still striving to develop various strategies to reinforce the existing physical properties of natural fibers or endow them with new exciting properties (Li, *et al.*, 2022, Liu, *et al.*, 2022, Leow, *et al.*, 2022, Sugiarto, *et al.*, 2022). For example, chemical treatment, such as grafting or modifying with desired functional groups (Thakur, *et al.*, 2014, Zeng, *et al.*, 2022) is a popular approach to improve the physical properties of cellulose-based natural fibers. On the other hand, the incorporation of functional nanomaterials (e.g., metal nanoparticles(Castellanos, *et al.*, 2012, Dong and Hinestroza, 2009), or metal oxides (Dolez, *et al.*, 2017)) has been emerging as a promising strategy to introduce bespoke features to natural fibers, such as antimicrobial, flame retardancy, UV-protection, and fluorescence properties.

Fluorescence switching materials are a class of smart material that can change their fluorescence color in response to remote light stimulation (Wei, *et al.*, 2018). They have received considerable research interests due to their versatility in a wide range of applications, such as optoelectronics, information storage, biological sensing and imaging, and anti-counterfeiting etc. (Huang, *et al.*, 2019, Qi, *et al.*, 2017, Zheng, *et al.*, 2022). A typical fluorescence switching material relies on organic molecules with photochromic moieties (e.g., azobenzene, dithienylethenes, fulgides, and spiropyrans) (Zhang, *et al.*, 2021, Yang, *et al.*, 2022), whose absorptions/emissions changes due to structure transformation induced by light. As very few photochromic molecules are simultaneously fluorescent, fluorescence switching

materials are more commonly prepared by conjugation of a fluorophore to a photochromic molecule, which works based on the Föster resonance energy transfer (FRET) mechanism (Dubertret, *et al.*, 2001, Lilley and Wilson, 2000, Zhang, *et al.*, 2021). The performance of resultant fluorescence switching material is optimized by modulating the spectral overlapping and the distance between the fluorophore and photochromic moiety, which usually involves cumbersome synthesis and laborious surface engineering.

Here, we report the facile preparation of a fluorescence switchable composite material simply constructed by fluorescent gold nanoclusters (AuNC) and renewable natural fibers. AuNC is a special type of gold nanoparticles consisting of tens to a hundred Au atoms and with a diameter less than 3 nm (Yu, *et al.*, 2013, Liu, *et al.*, 2022, Li, *et al.*, 2022, Wang, *et al.*, 2022, Li, *et al.*, 2022). Due to the influence of strong quantum confinement effect in this size regime, AuNC exhibit unique physical and chemical properties that are distinct from their larger counterparts, such as enhanced fluorescence (Qian, *et al.*, 2022, McCoy, *et al.*, 2013, Shi, *et al.*, 2017, Kim, *et al.*, 2020, Liu, *et al.*, 2021). The key design of this study was to utilize delignified natural fibers harvested from coconut husk (or coir) as a reducing and nucleating agent for the in-situ formation of AuNC (the obtained composite material is denoted as coir@AuNC hereafter). The delignified coir has a cellulose-dominant backbone with abundant hydroxyl groups, which were activated at an elevated temperature (~75°C) to facilitate the reduction of Au salts and formation of AuNC (with the assistance of a small bio-occurring tripeptide *L*-glutathione). More importantly, the delignified coir which showed intrinsic green emission was switched into an orange-emissive composite after the in-situ formation of AuNC. The fluorescence switching property of the coir@AuNC was attributed to fluorescence resonance energy transfer (FRET) from the substrate (delignified coir) to AuNC despite their large disparity at first glance. We had carefully characterized the fibrous materials before and after immobilization of AuNC and determined the key parameters during the FRET process.

2. Materials and methods

2.1.Materials

Sodium chlorite ($NaClO_2$, technical grade, 80.0%), Sodium Acetate (CH_3COONa, ACS reagent, ≥99.0%), acetic acid (CH_3COOH, glacial, ACS reagent, ≥99.7%), L-glutathione reduced (γ-glu-cys-gly, GSH, ≥98.0%), gold (III) chloride trihydrate ($HAuCl_4 \cdot 3H_2O$, ACS reagent, ≥49.0% Au basis) were purchased from Sigma-Aldrich and used as received. Deionized (DI) water with a resistivity of 18.2 MΩ was used as a common solvent throughout this study.

2.2.In-situ delignification of coconut fibers

The delignification solution was prepared by dissolving sodium chlorite ($NaClO_2$) in acetate buffer (0.1 M, pH 4.6) at a concentration of 1 wt%. Prior to delignification, raw coconut fibers (coir) were washed with DI water thrice to remove surface impurities, and oven-dried at 105 °C overnight to remove any moisture. In a typical delignification process, the oven-dried coir (2 g) was immersed in a 200 mL of delignification solution and left to stand for 16 h at 80 °C under gentle stirring (50 rpm). The delignified fibers were then separated by filtration and washed with DI water continuously until a neutral pH was reached.

2.3.In-situ synthesis of coir@AuNC composites

In a typical synthesis, 100 mg of delignified coir was soaked in a 30-mL glass vial containing 10 mL ultrapure water, followed by sequentially adding aqueous solutions of GSH (3 mL, 20 mM) and $HAuCl_4$ (2 mL, 20 mM). After mixing thoroughly using a vortex mixer, the vial was sealed airtight and placed inside a 75 °C oven for 24 h. For comparison, samples without adding either GSH or $HAuCl_4$, or with coir only were also subjected to the similar heating treatment. After 24 h, the samples were recovered, washed by DI water thrice, and freeze-dried for further study.

2.4.Characterizations

UV-vis spectra were measured on a Shimadzu UV-2450 spectrometer. Steady-state photoluminescence spectra (PL) were measured on a FLAME-S-XR1-ES spectrometer coupling with a 405 nm light source (Ocean Insights). X-ray photoelectron spectroscopy (XPS) measurements were performed on a PHI Quantera SXM Scanning XPS Microprobe. Scanning electron microscopy (SEM) images were recorded on a JEOL JSM6700F field emission scanning electron microscope operating at 5 kV. Transmission electron microscopy (TEM) was done on a FEI Titan 80-300 TEM at an accelerating voltage of 200kV. Cross-sections of ~200 nm thickness of the coir@AuNC were made by cutting a fiber embedded in epoxy resin using an ultra-microtome (Leica Ultracut UCT) at room temperature. Thermogravimetric analysis (TGA) was done using a TA Instruments TGA Q500 analyzer. X-ray diffraction (XRD) spectra were recorded on a Bruker D8 ADVANCE diffractometer. Fluorescence lifetime was measured on a MicroTime 200 microscopy platform. Photoluminescence quantum efficiency (PLQE) was determined using a three-measurement method (de Mello, *et al.*, 1997, Leyre, *et al.*, 2014) with a setup consisting of a 405 nm violet and blue alignment laser diode, a 6-in integrating sphere, and a QE Pro high-performance spectrometer (Ocean Insights). Specifically, the number of photons in the excitation wavelength region was measured (L_a) in the first measurement. The second measurement determines the number of photons in the incident wavelength region (L_b) and the number of photons in the emission wavelength region (P_b), with the sample present in the integrating sphere but out of the path of the incident beam. In the last measurement, the number of photons in the incident wavelength region (L_c) and the number of photons in the emission wavelength region (P_c) were determined with the sample present in the integrating sphere and directly illuminated by the incident beam. The PLQE value was then determined using the following equation (Equation 1):

$$PLQE = \frac{P_c - (1-A)P_b}{L_a A} \quad (1)$$

Where $A = 1 - L_c/L_b$ is the direct absorption.

2.5. Calculation of FRET efficiency (E), rate constant (k_T), the Förster radius (R_0) and the distance between donor-acceptor pair (R_{DA})

The FRET efficiency (E) is correlated with the lifetime of donor (τ_D) and the rate constant (k_T) in the Equation (2) below (Bajar, *et al.*, 2016, Vogel, *et al.*, 2014):

$$E = 1 - \frac{\tau_{DA}}{\tau_D} = \frac{k_T}{\frac{1}{\tau_D} + k_T} = \frac{1}{R_0^6 + R_{DA}^6} \quad (2)$$

By using the values of τ_D and τ_{DA} determined in Fig. 4b and Table S2, E is determined to be 6.4%. With the known value of E, the energy transfer rate constant k_T is estimated to be 2.74 $\times 10^7$ s^{-1}. The Förster radius (R_0, in nm) is then calculated using Equation (3) (Bajar, *et al.*, 2016):

$$R_0 = 0.02108\ (\kappa^2 \phi_D n^{-4} J)^{\frac{1}{6}} \quad (3)$$

where κ^2 is the interdipole orientation factor and assumed to be 2/3, ϕ_D is the fluorescence quantum efficiency of donor in the absence of acceptor (3.3%), n is the refractive index of medium (approximately 1 for atmosphere), and J is the overlap integral of the donor emission and acceptor absorption spectra (which is 1.26×10^{14} M^{-1} cm^{-1} nm^4 estimated from Fig. 4a). By applying values of κ^2, ϕ_D, n, J in Equation 3, we get R_0 to be 2.50 nm. With known value of R_0, R_{DA} is determined to be 1.53 nm.

3. Results and discussion

Fig. 1a showed the typical two-step synthesis of the AuNC on coir composite material (denoted as coir@AuNC hereafter for convenience of reference). In the first step, the raw coir was

160 treated in a buffered solution of sodium chlorite ($NaClO_2$, 1 wt% in 0.1 M acetate buffer, pH
161 4.6) at 80 °C to give the delignified coir (item ***1***). This delignification process thoroughly
162 bleached away the brown pigments in the raw coir and yield a porous structure in the delignified
163 coir (Fig. S1). In the second step, the delignified coir (item ***1***) was immersed in a mixture
164 solution of *L*-glutathione (GSH) and gold (III) salts and placed inside a 75 °C oven for 24 h to
165 yield the coir@AuNC composite material (item ***2***, more details are available in Section 2.2 and
166 2.3). Interestingly, the initially non-fluorescent raw coir (Fig. S2) was able to give off green
167 emissions under UV irradiation after the delignification treatment (Fig. 1b inset, item ***1***). It has
168 been reported that cellulose can show blue emissions upon UV irradiation due to abundant
169 hydroxyl groups forming hydrogen bonds to rigidify molecular conformations (Zeng, *et al.*,
170 2022). On the other hand, lignin are rich in aromatic subunits which may serve as centers of
171 chromophore and fluorophore (Moreno and Sipponen, 2020, Sugiarto, *et al.*, 2022). Indeed
172 green-emitting lignin nanospheres have been used for photodynamic therapy applications
173 recently (Paul, *et al.*, 2021). Considering lignin cannot be completely removed by chlorite
174 treatment, we believe that small amount of lignin remaining in the delignified coir was the
175 source of the observed green emission where its fluroescence was further enhanced by the
176 rigidification effect from the hydrogen bonds in the cellulose matrix.

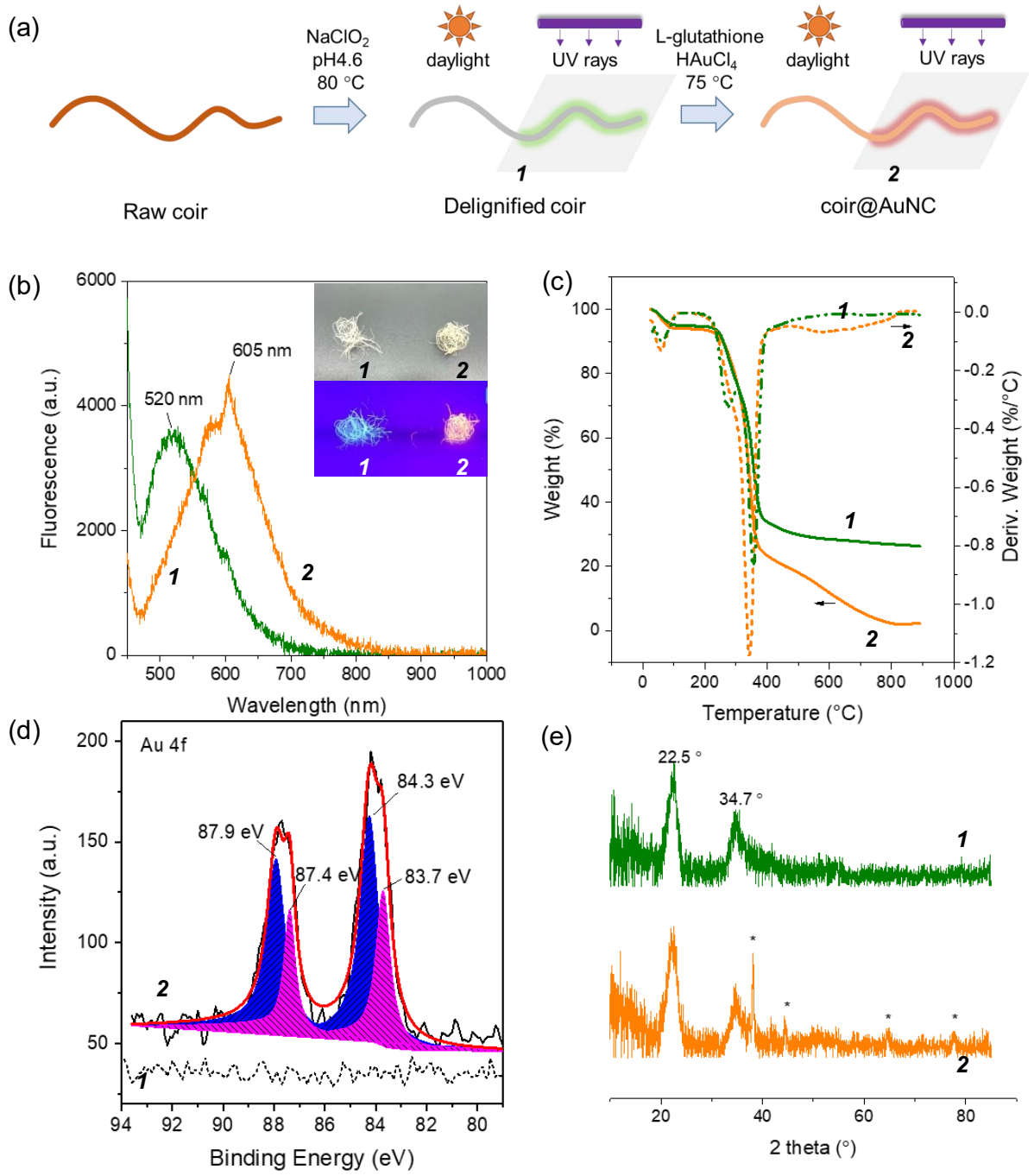

Fig. 1 (a) Schematic diagram of the formation process of emissive coir coated with AuNC. The color code illustrates the appearance of delignified coir only and coir coated with AuNC under daylight and UV irradiation. (b) Fluorescence spectra (λ_{ex} = 405 nm) of the delignified coir (***1***) and coir coated with AuNC (***2***). (Inset) Digital photos of the delignified coir (***1***) and coir coated with AuNC (***2***) under day light (top) and in the dark under UV light (bottom). (c) TGA and DTG curves of the delignified coir (***1***) and coir coated with AuNC (***2***). (d) High resolution XPS spectra of Au 4f for delignified coir and coir coated with AuNC, respectively. (e) XRD spectra of the delignified coir (***1***) and coir coated with AuNC (***2***). The stars indicate the (111), (200), (220), and (311) facets of the formed AuNC particles.

More interestingly, the formed coir@AuNC composite material demonstrated orange emissions under UV irradiation (Fig. 1b inset, item ***2***), which was distinctly different from the green emissions of the delignified coir fibers. The fluorescence spectrum of delignified coir fibers (***1***) showed a peak centered at 520 nm while that of coir@AuNC (***2***) exhibited a peak at 605 nm (λ_{ex} = 405 nm) (Fig. 1b). Thermogravimetric analysis (TGA) of delignified coir fibers (***1***) and coir@AuNC (***2***) confirmed the successful loading of AuNC, as evidenced by the merging of two transition ranges (ca. 205–310 °C and 310–420 °C) initially observed for delignified coir fibers and the emergence of another transition range above 450 °C on the TGA curve of coir@AuNC (Fig. 1c and Table S1). It is worthy to mention that the decomposition of coir was more thorough for the coir@AuNC composite, which might be attributed to the catalytic properties of ultrasmall gold nanoparticles ((Kim, *et al.*, 2020, Wang, *et al.*, 2022)). The successful loading of AuNC was also supported by the high resolution XPS spectra of delignified coir fibers (***1***) and coir@AuNC (***2***) (Fig. 1d). Further deconvolution of the $Au4f_{7/2}$ spectrum into Au(I) and Au(0) components (with binding energy of 84.3 and 83.7 eV, respectively) translated into ~64% Au(I) of all Au atoms in the formed AuNC – a typical physical property for ultrasmall AuNC (Yu, *et al.*, 2014). X-ray diffraction (XRD) studies revealed the preservation of crystalline cellulose (Nang An, *et al.*, 2020, Tomczak, *et al.*, 2007) after delignification, as evidenced by two evident peaks at 2θ = 22.5° and 34.7 ° on both XRD spectra of the raw (Fig. S3) and the delignified coir (Fig. 1e, item ***1***). On the other hand, a set of new peaks at 2θ = 38.2°, 44.3°, 64.6° and 77.6° were observed on the XRD spectrum of coir@AuNC, which matched the *fcc* stacking of gold nanoparticles (Fig. 1e, item ***2***). Previous reports of powder X-ray diffraction pattern of thiolate-protected AuNC only show a broad peak at 2θ = 30–40° (Qian and Jin, 2009, Nimmala, *et al.*, 2013, Yao, *et al.*, 2015). We reasoned that the deviation in this study might come from the immobolization of AuNC on the bleached coir (in stead of free thiolate protection). The crystallinity surface cellulose microfibrils could

induce the prefential stacking of gold atoms in the current study. It is interesting to note that in a previous study ultrasmall gold nanoparticles (~1.7 nm) synthesized in ionic liquids also show similar XRD patterns (Wang, *et al.*, 2008). Last but not least, the formation of AuNC with a diameter of 1-2 nm was also confirmed by TEM. A typical fiber of coir@AuNC composite was microtome cut into thin (~200 nm in thickness) slices perpendicualrly and the cross section area was observed under the TEM. The bright filed TEM iamges showed that the lacuna (hole) of the composite was several micrometers across (Fig. 2a). A thin layer of tens of nanometers with higher contrast (dark) as compared to the cellulose matrix indicated the formation of tiny particles around the inner surface. High-angle annular dark field scanning TEM (HAADF-STEM) images (Fig. 2b-d) were recorded to further examine the size of the formed AuNC as HAADF-STEM images are more sensitive to atomic mass. The as-formed AuNC around the inner surface of the lacuna appeared as a white layer in the low magnification HAADF-STEM images (Fig. 2b and c). The high resolution HAADF-STEM image clearly showed that the as-formed AuNC are indeed very small with a diameter less than 3 nm (Fig. 2d).

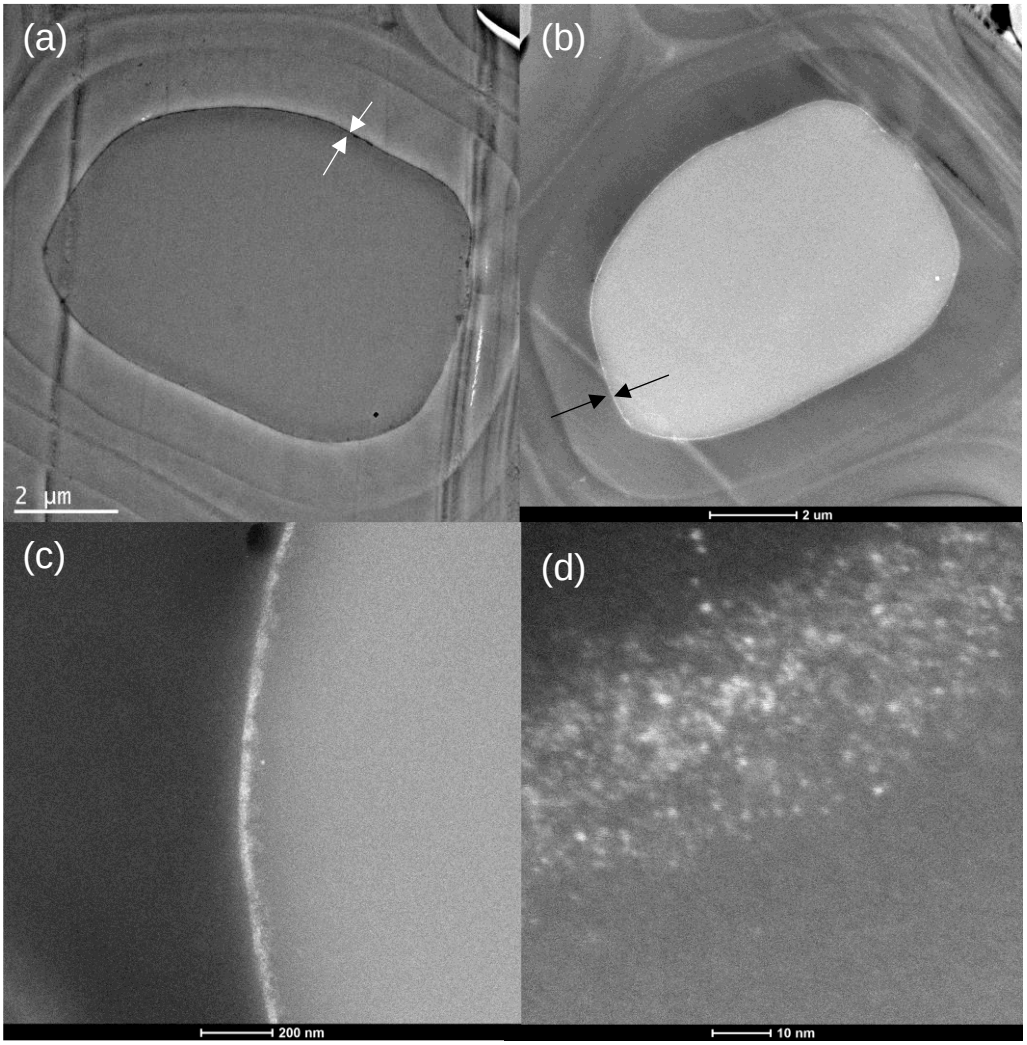

Figure 2. (a) Bright field TEM and (b-d) high-angle annular dark field scanning TEM (HAADF-STEM) images observed for the cross section of coir@AuNC composite.

Several control experiments had been carried out to better comprehend the formation of the orange-emitting coir@AuNC. First, hydrothermal treatment of the delignified coir alone at 75 °C for 24 h did not produce any orange-emitting species. The delignified coir remained in pale yellow and emitted green light upon UV irradiation (Fig. 3a, left panel). The zoomed-in scanning electron micrographs near one typical pit and the lacuna at the cross section showed the surface of the delignified coir was clean (Fig. 3a, middle and right panels). Second, hydrothermal treatment of the delignified coir with GSH did not change the fluorescence of the

delignified coir (Fig. 3b, left panel). However, a layer of film/coating seemed to be formed on the surface of the delignified coir, possibly due to the interaction of GSH with the cellulose backbone of the coir (Fig. 3b, middle and right panels). On the other hand, hydrothermal treatment of the delignified fibers with Au salts led to brown coir with no orange emissions (Fig. 3c, left panel). The darker color of the coir indicated the formation of larger Au nanoparticles on the surface of the resultant fibers. Because the major component of delignified coir was cellulose that consisted of long chains of D-glucose subunits with abundant hydroxyl groups, the delignified coir can serve as both reducing and nucleating agent to facilitate the growth of Au nanoparticles, resembling the biomineralization phenomenon in nature (Dickerson, *et al.*, 2008). SEM images showed the fiber surface was decorated with various-sized (tens to hundreds of nanometers), plate-like triangles and hexagons (Fig. 3c, middle), while the lacuna area was mainly coated with truncated octahedrons (Fig. 3d, right). This observation suggested that the hydroxyl groups preferentially bound to the (111) facet of the Au twinned crystal seeds formed at the initial stage, leading to the preferential growth of (100) facet to form large and thin platelets on the coir surface (Krauss, *et al.*, 2018). Lastly, when both GSH and Au salts were present, the size of Au nanoparticles were greatly reduced to form AuNCs (less than 3 nm), as evidenced by the unique orange emission of the coir@AuNC composite (Fig. 3d, left panel). No big particles (i.e., of tens to hundreds of nanometers) were observed on the SEM images of the surface and cross section area of the composite fiber (Fig. 3d, middle and right panel), which is consistent with the TEM images of the cross section area of the composite fiber (Fig. 2). It should be mentioned that AuNC was also formed in the bulk solution away from coir (Fig. S4). However, the clear difference in their fluorescence spectra revealed the interaction of AuNC formed on coir with the fiber. We believe this difference roots in the dual role of GSH in the current study, which not only restricts the further growth of AuNC but also anchors the formed AuNC on the coir backbone. Indeed, the high resolution

XPS spectrum of S2p of the coir@AuNC showed only a small portion of S (~18%) is in the thiolate form available to interact with AuNC (Fig. S5). The binding of GSH to the coir backbone may be achieved by C-N or C-S interactions as revealed by the high resolution XPS spectrum of C1s (Fig. S6).

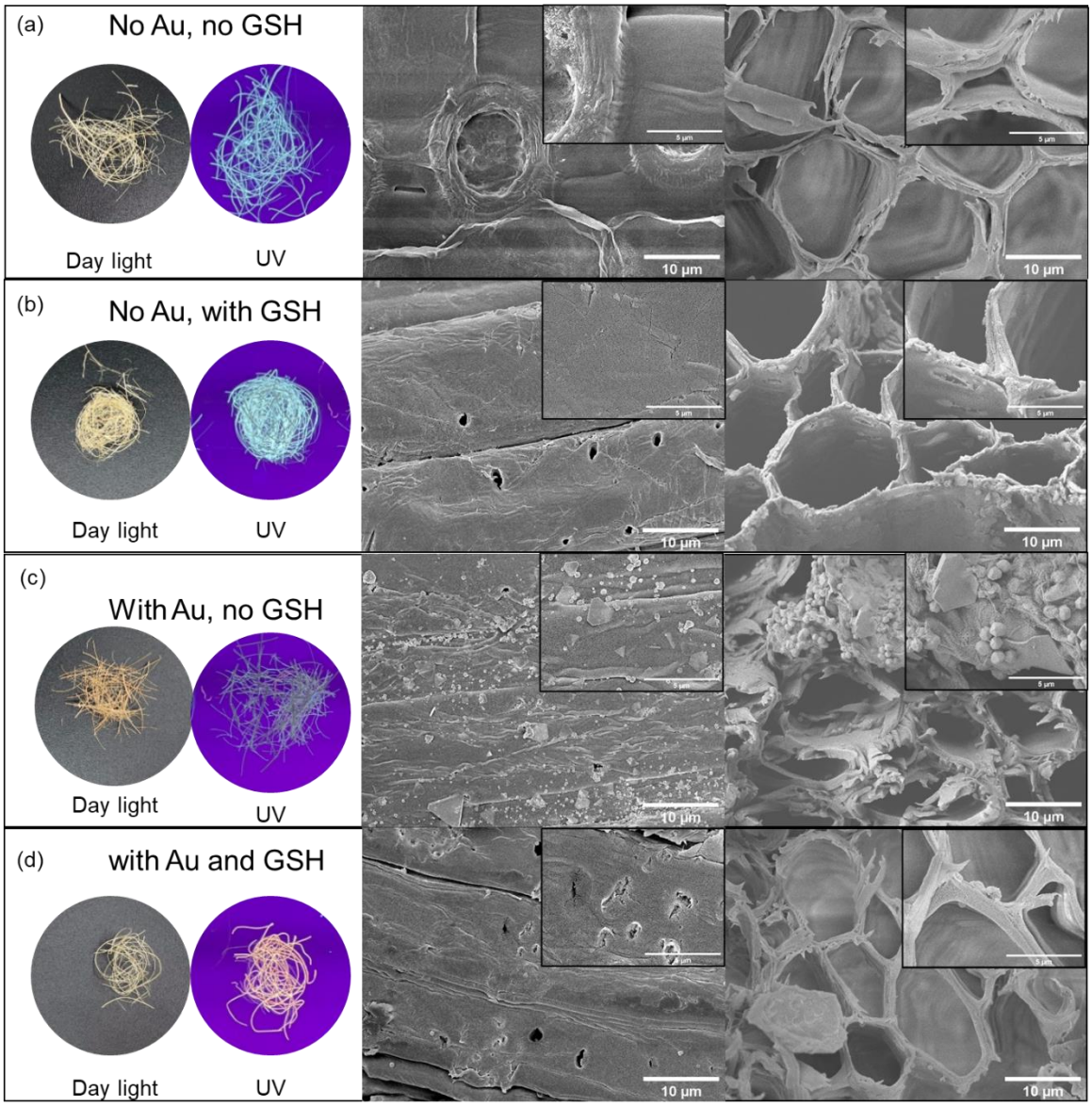

Fig. 3 Digital photos of the final products prepared at different conditions under day light and UV light (left), and corresponding SEM images of the fiber surface (middle) and cross-sections (right). (a) Fiber only, no GSH, no Au. (b) Fiber with GSH. (c) Fiber with Au salts. (d) Fiber with Au salts and GSH.

When a pair of fluorophores are 1) in proximity, 2) arranged with appropriate orientation, and 3) the fluorescence spectrum of one fluorophore overlaps with the excitation spectrum of the other, the fluorescence energy of the former fluorophore (as donor) will be absorbed by the second (as acceptor) to induce or enhance its fluorescence. This phenomenon has been well known as Forster resonance energy transfer (FRET) (Zhang, *et al.*, 2021, Oh, *et al.*, 2016). At first glance, the two entities, i.e., AuNC and delignified coir, showed distinct difference in material type, morphology, and dimension. However, as the size of formed AuNC was less than 3 nm, the distance from the coir backbone should be small enough to allow for energy transfer and possible fluorescence switching. As a first check, we employed the UV-vis absorption spectrum of AuNC in the supernatant to mimic the AuNC formed on coir and found that the UV-vis absorption spectrum of AuNC overlapped with the fluorescence spectrum of coir (Fig. 4a). We then proposed a FRET model in which the delignified coir served as donor fluorophore while the deposited AuNC functioned as the acceptor to describe the fluorescence switching of coir upon in-situ formation of AuNC. The simplified Jablonski energy diagram was shown Fig. 4c.

The FRET efficiency (E), rate constant (k_T), the Förster radius (R_0) and the distance between donor-acceptor pair (R_{DA}) are important parameters used to describe the resonance energy transfer process. We first studied the time-resolved photoluminescence decay profiles of the delignified coir and the coir@AuNC, which were used to estimate the lifetimes of the emitting species (Fig. 4b). The apparent lifetime of the delignified coir in the absence (τ_D) and presence of AuNC acceptor (τ_{DA}) was 2.50 and 2.34 ns, respectively (Table S2). The apparent lifetime of AuNC alone was measured to be 514.19 ns by applying a 600 nm longpass filter, which was consistent with previously reported lifetimes of AuNCs (Li, *et al.*, 2022, Yu, *et al.*, 2014). We then measured the absolute fluorescence quantum yield of delignified coir in the absence of AuNC and calculated the values of E, k_T, R_0 and R_{DA} using the method described previously

(Bajar, *et al.*, 2016, Vogel, *et al.*, 2014) (detailed calculations are available in Section 2.5). As listed in Fig. 4d, the FRET efficiency (E) from delignified coir to AuNC was 6.4% and the rate constant k_T was 2.74 $\times 10^7$ s^{-1}. Notably, the calculated R_0 is 2.50 nm, which is shorter than commonly used fluorescent protein FRET pairs (Bajar, *et al.*, 2016). Accordingly, the distance between AuNC and the delignified coir (R_{DA}) was estimated to be 1.53 nm, which agreed with the particle size of AuNC. A shorter R_0 may arise from the relatively small spectral overlap and possibly mismatch of AuNC and delignified coir in dimension (which may affect the orientation of the donor-acceptor pair). Nevertheless, the fluorescence energy transfer between the AuNC and the delignified coir can still be described using the classic FRET model despite their dissimilarity in material type, morphology, and geometric dimension.

(a)

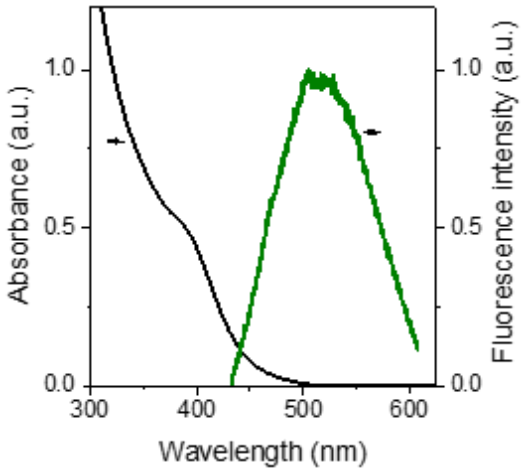

(b)

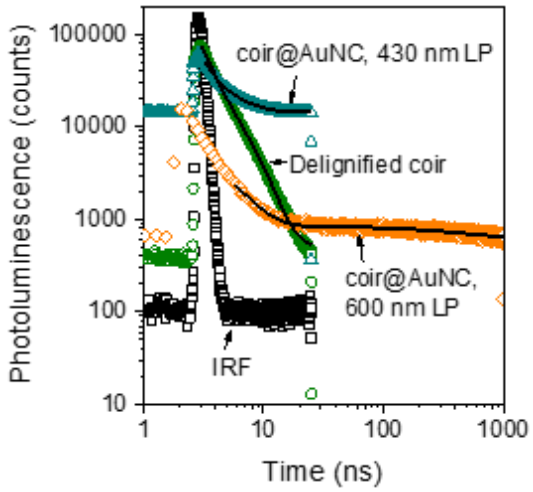

(c)

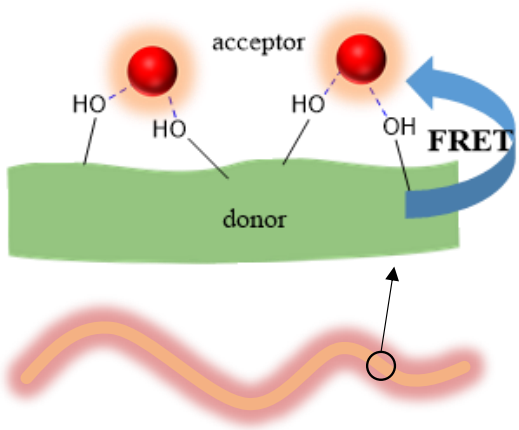

(d)

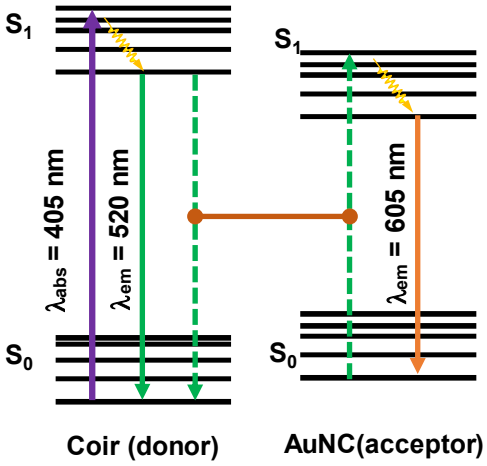

Parameters	Physical meaning	Values
E	Efficiency of Resonance energy transfer	6.4%
k_T	Rate constant of FRET	2.74 $\times 10^7$ s^{-1}
R_0	at which 50% FRET occurs	2.50 nm
R_{DA}	Distance of donor and acceptor	1.53 nm

Fig. 4 (a) Overlap of the UV-vis spectrum of AuNC and the photoluminescence spectrum of delignified coir. (b) Time-resolved photoluminescence decay profiles of the delignified coir and the coir@AuNC composite. (c) Schematic illustration of FRET from the delignified coir to AuNC in the coir@AuNC composite and its simplified Jablonski energy diagram. (d) Summary of key values calculated to describe the energy transfer process.

FRET is extremely sensitive to the distance of the donor-acceptor pair. Particularly, the Förster radius (R_0) is proportional to the inverse of the 4th power of refractive index ($R_0 \propto n^{-4}$). The variation of medium between the donor and acceptor may change R_0 and thus greatly alter E. For example, if the coir@AuNC composite was soaked in a certain type of solvent (e.g., water with a refractive index of 1.33), R_0 will decreased to 31% (i.e., 1.33^{-4}) of that in dry state, which made the FRET more difficult to occur. Indeed, we soaked the coir@AuNC composite in several common solvents with refractive indices greater than unity (Table S3) and observed that the fluorescence peak all shifted from 605 nm to 520 nm (Fig. 5a). This observation further confirmed the fluorescence energy transfer from the coir to AuNC as blocking of this process leads to fluorescence recovery of the coir backbone (λ_{em} = 520 nm). This ratiometric fluorescence response of coir@AuNC may be used as either a dryness indicator or stimuli (solvent)-responsive sensor based on the ratio of fluorescence intensity at different peaks (Fig. 5b). Notably, this solvent-induced fluorescence change was also reversible (Fig. S7).

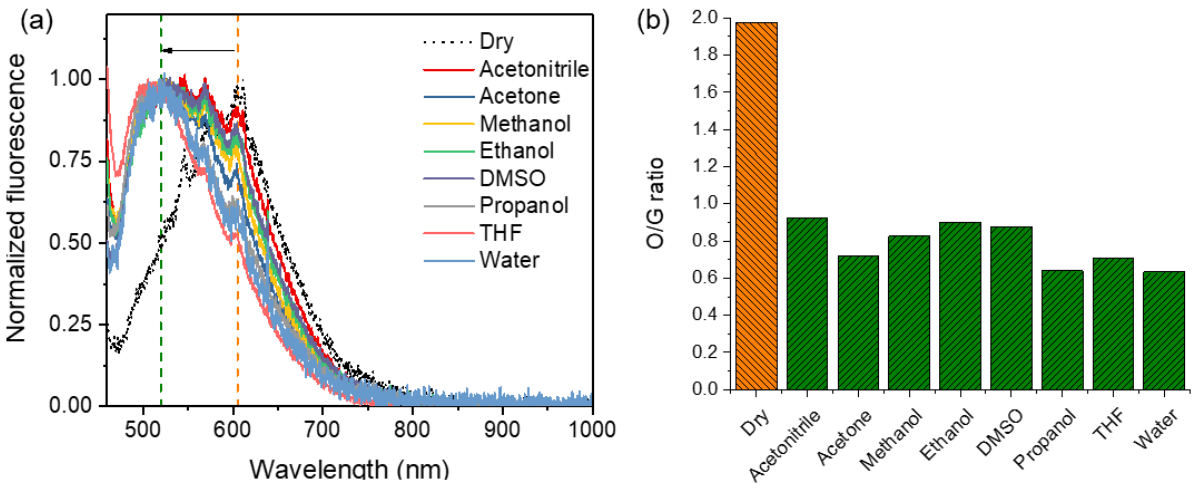

Fig. 5 (a) Normalized photoluminescence spectra of the coir@AuNC in the presence of different solvents. (b) Ratiometric fluorescence (as O/G where O and G represent the fluorescence intensity at 605 nm and 520 nm, respectively) of the coir@AuNC in the presence of different solvents.

4. Conclusion

In summary, we present a unique fluorescence switchable composite material formed by in-situ formation of ultrasmall Au nanoclusters on coconut fibers (coir@AuNC). Coconuts fibers that were delignified by a chemical method were used as a reducing and nucleating agent for the synthesis of AuNC. The hydroxyl groups of cellulose backbone of delignified coir facilitated the reduction of Au salts and growth of AuNC. The role of the bio-occurring tripeptide (*L*-glutathione) present during the Au NC synthesis was identified to restrict the size of formed AuNC and secure them on the surface of coconut fibers. More interestingly, the initial green emission of delignified coir was switched to orange emission of the obtained composite material. The Förster resonance energy transfer (FRET) from the delignified coir to AuNC has been outlined to explain the observed fluorescence switching with several critical parameters being determined, such as FRET efficiency, Förster radius and the rate constant of FRET. The distance-sensitive FRET process was also confirmed by varying the medium between the formed AuNC and delignified coir, which highlighted the potential uses in stimuli-responsive sensor applications. More importantly, this study established a new method of endowing unique functionalities to natural fibers and provided a more facile and sustainable alternative means to prepare fluorescence switching materials. Considering that metal NC can be rationally designed for a wide variety of properties, this method is potentially versatile to create functional composite natural materials for diverse uses in energy, catalysis, and biomedical applications.

Conflicts of interest

There are no conflicts to declare.

Acknowledgement

This research is supported by the Agency for Science, Technology and Research (A*STAR), <Project No. CDA 202D800033, AME Programmatic Funds A18A1b0045> and SERC Central Research Fund.

References

Silva, G., Kim, S., Aguilar, R. and Nakamatsu, J., 2020. *Natural Fibers as Reinforcement Additives for Geopolymers – a Review of Potential Eco-Friendly Applications to the Construction Industry*. *Sustain. Mater. Technol.*, **23**, e00132.https://doi.org/10.1016/j.susmat.2019.e00132.

Hasan, K. M. F., Horváth, P. G., Bak, M. and Alpár, T., 2021. *A State-of-the-Art Review on Coir Fiber-Reinforced Biocomposites*. *RSC Adv.*, **11**, 10548-10571.10.1039/D1RA00231G.

Berardi, U. and Iannace, G., 2015. *Acoustic Characterization of Natural Fibers for Sound Absorption Applications*. *Build. Environ.*, **94**, 840-852.https://doi.org/10.1016/j.buildenv.2015.05.029.

Li, Z., Chen, C., Xie, H., Yao, Y., Zhang, X., Brozena, A., Li, J., Ding, Y., Zhao, X., Hong, M., Qiao, H., Smith, L. M., Pan, X., Briber, R., Shi, S. Q. and Hu, L., 2022. *Sustainable High-Strength Macrofibres Extracted from Natural Bamboo*. *Nat. Sustain.*, **5**, 235-244.10.1038/s41893-021-00831-2.

Liu, J., Kong, T. and Xiong, H.-M., 2022. *Mulberry-Leaves-Derived Red-Emissive Carbon Dots for Feeding Silkworms to Produce Brightly Fluorescent Silk*. *Adv. Mater.*, **34**, 2200152.https://doi.org/10.1002/adma.202200152.

Leow, Y., Sequerah, V., Tan, Y. C., Yu, Y., Peterson, E. C., Jiang, C., Zhang, Z., Yang, L., Loh, X. J. and Kai, D., 2022. *A Tough, Biodegradable and Water-Resistant Plastic Alternative from Coconut Husk*. *Compos. Part B Eng.*, **241**, 110031.https://doi.org/10.1016/j.compositesb.2022.110031.

Sugiarto, S., Pong, R. R., Tan, Y. C., Leow, Y., Sathasivam, T., Zhu, Q., Loh, X. J. and Kai, D., 2022. *Advances in Sustainable Polymeric Materials from Lignocellulosic Biomass*. *Mater. Today Chem.*, **26**, 101022.https://doi.org/10.1016/j.mtchem.2022.101022.

Thakur, V. K., Thakur, M. K. and Gupta, R. K., 2014. *Graft Copolymers of Natural Fibers for Green Composites*. *Carbohydr. Polym.*, **104**, 87-93.https://doi.org/10.1016/j.carbpol.2014.01.016.

Zeng, M., Li, T., Liu, Y., Lin, X., Zu, X., Mu, Y., Chen, L., Huo, Y. and Qin, Y., 2022. *Cellulose-Based Photo-Enhanced Persistent Room-Temperature Phosphorescent Materials by Space Stacking Effects*. *Chem. Eng. J.*, **446**, 136935.https://doi.org/10.1016/j.cej.2022.136935.

Castellanos, L. J., Blanco-Tirado, C., Hinestroza, J. P. and Combariza, M. Y., 2012. *In Situ Synthesis of Gold Nanoparticles Using Fique Natural Fibers as Template*. *Cellulose*, **19**, 1933-1943.10.1007/s10570-012-9763-8.

Dong, B. H. and Hinestroza, J. P., 2009. *Metal Nanoparticles on Natural Cellulose Fibers: Electrostatic Assembly and in Situ Synthesis*. *ACS Appl. Mater. Interfaces*, **1**, 797-803.10.1021/am800225j.

Dolez, P. I., Arfaoui, M. A., Dubé, M. and David, É., 2017. *Hydrophobic Treatments for Natural Fibers Based on Metal Oxide Nanoparticles and Fatty Acids*. *Procedia Eng.*, **200**, 81-88.https://doi.org/10.1016/j.proeng.2017.07.013.

Wei, P., Zhang, J.-X., Zhao, Z., Chen, Y., He, X., Chen, M., Gong, J., Sung, H. H. Y., Williams, I. D., Lam, J. W. Y. and Tang, B. Z., 2018. *Multiple yet Controllable Photoswitching in a Single Aiegen System*. *J. Am. Chem. Soc.*, **140**, 1966-1975.10.1021/jacs.7b13364.

Huang, G., Xia, Q., Huang, W., Tian, J., He, Z., Li, B. S. and Tang, B. Z., 2019. *Multiple Anti-Counterfeiting Guarantees from a Simple Tetraphenylethylene Derivative – High-Contrasted and Multi-State Mechanochromism and Photochromism*. *Angew. Chem. Int. Ed.*, **58**, 17814-17819.https://doi.org/10.1002/anie.201910530.

Qi, Q., Li, C., Liu, X., Jiang, S., Xu, Z., Lee, R., Zhu, M., Xu, B. and Tian, W., 2017. *Solid-State Photoinduced Luminescence Switch for Advanced Anticounterfeiting and Super-Resolution Imaging Applications*. *J. Am. Chem. Soc.*, **139**, 16036-16039.10.1021/jacs.7b07738.

Zheng, Y., Meana, Y., Mazza, M. M. A., Baker, J. D., Minnett, P. J. and Raymo, F. M., 2022. *Fluorescence Switching for Temperature Sensing in Water*. *J. Am. Chem. Soc.*, **144**, 4759-4763.10.1021/jacs.2c00820.

Zhang, X., Ma, Z., Li, X., Qian, C., Liu, Y., Wang, S., Jia, X. and Ma, Z., 2021. *Multiresponsive Tetra-Arylethene-Based Fluorescent Switch with Multicolored Changes: Single-Crystal Photochromism, Mechanochromism, and Acidichromism*. *ACS Appl. Mater. Interfaces*, **13**, 40986-40994.10.1021/acsami.1c12187.

Yang, R., Ren, X., Mei, L., Pan, G., Li, X.-Z., Wu, Z., Zhang, S., Ma, W., Yu, W., Fang, H.-H., Li, C., Zhu, M.-Q., Hu, Z., Sun, T., Xu, B. and Tian, W., 2022. *Reversible Three-Color Fluorescence Switching of an Organic Molecule in the Solid State Via "Pump–Trigger" Optical Manipulation*. *Angew. Chem. Int. Ed.*, **61**, e202117158.https://doi.org/10.1002/anie.202117158.

Dubertret, B., Calame, M. and Libchaber, A. J., 2001. *Single-Mismatch Detection Using Gold-Quenched Fluorescent Oligonucleotides*. *Nat. Biotechnol.*, **19**, 365-370.10.1038/86762.

Lilley, D. M. J. and Wilson, T. J., 2000. *Fluorescence Resonance Energy Transfer as a Structural Tool for Nucleic Acids*. *Curr. Opin. Chem. Biol.*, **4**, 507-517.https://doi.org/10.1016/S1367-5931(00)00124-1.

Zhang, Y., Xu, H., Yang, Y., Zhu, F., Pu, Y., You, X. and Liao, X., 2021. *Efficient Fluorescence Resonance Energy Transfer-Based Ratiometric Fluorescent Probe for Detection of Dopamine Using a Dual-Emission Carbon Dot-Gold Nanocluster Nanohybrid*. *J. Photochem. Photobiol. A: Chem.*, **411**, 113195.https://doi.org/10.1016/j.jphotochem.2021.113195.

Yu, Y., Yao, Q., Luo, Z., Yuan, X., Lee, J. Y. and Xie, J., 2013. *Precursor Engineering and Controlled Conversion for the Synthesis of Monodisperse Thiolate-Protected Metal Nanoclusters*. *Nanoscale*, **5**, 4606-4620.10.1039/C3NR00464C.

Liu, Y., Liu, Y., Zhang, J., Zheng, J., Yuan, Z. and Lu, C., 2022. *Catechin-Inspired Gold Nanocluster Nanoprobe for Selective and Ratiometric Dopamine Detection Via Forming Azamonardine*. *Spectrochim. Acta A Mol. Biomol. Spectrosc.*, **274**, 121142.https://doi.org/10.1016/j.saa.2022.121142.

Li, J.-J., Liu, Z., Guan, Z.-J., Han, X.-S., Shi, W.-Q. and Wang, Q.-M., 2022. *A 59-Electron Non-Magic-Number Gold Nanocluster Au99(C≡Cr)40 Showing Unexpectedly High Stability*. *J. Am. Chem. Soc.*, **144**, 690-694.10.1021/jacs.1c11643.

Wang, S., Tang, L., Cai, B., Yin, Z., Li, Y., Xiong, L., Kang, X., Xuan, J., Pei, Y. and Zhu, M., 2022. *Ligand Modification of Au25 Nanoclusters for near-Infrared Photocatalytic Oxidative Functionalization*. *J. Am. Chem. Soc.*, **144**, 3787-3792.10.1021/jacs.2c01570.

Li, Y., Song, Y., Zhang, X., Liu, T., Xu, T., Wang, H., Jiang, D.-e. and Jin, R., 2022. *Atomically Precise Au42 Nanorods with Longitudinal Excitons for an Intense Photothermal Effect*. *J. Am. Chem. Soc.*, **144**, 12381-12389.10.1021/jacs.2c03948.

Qian, S., Wang, Z., Zuo, Z., Wang, X., Wang, Q. and Yuan, X., 2022. *Engineering Luminescent Metal Nanoclusters for Sensing Applications*. *Coord. Chem. Rev.*, **451**, 214268.https://doi.org/10.1016/j.ccr.2021.214268.

McCoy, R. S., Choi, S., Collins, G., Ackerson, B. J. and Ackerson, C. J., 2013. *Superatom Paramagnetism Enables Gold Nanocluster Heating in Applied Radiofrequency Fields*. *ACS Nano*, **7**, 2610-2616.10.1021/nn306015c.

Shi, L., Zhu, L., Guo, J., Zhang, L., Shi, Y., Zhang, Y., Hou, K., Zheng, Y., Zhu, Y., Lv, J., Liu, S. and Tang, Z., 2017. *Self-Assembly of Chiral Gold Clusters into Crystalline Nanocubes of Exceptional Optical Activity*. *Angew. Chem. Int. Ed.*, **56**, 15397-15401.https://doi.org/10.1002/anie.201709827.

Kim, B., Seong, H., Song, J. T., Kwak, K., Song, H., Tan, Y. C., Park, G., Lee, D. and Oh, J., 2020. *Over a 15.9% Solar-to-Co Conversion from Dilute Co2 Streams Catalyzed by Gold Nanoclusters Exhibiting a High Co2 Binding Affinity*. *ACS Energy Lett.*, **5**, 749-757.10.1021/acsenergylett.9b02511.

Liu, Z., Wu, Z., Yao, Q., Cao, Y., Chai, O. J. H. and Xie, J., 2021. *Correlations between the Fundamentals and Applications of Ultrasmall Metal Nanoclusters: Recent Advances in Catalysis and Biomedical Applications*. *Nano Today*, **36**, 101053.https://doi.org/10.1016/j.nantod.2020.101053.

de Mello, J. C., Wittmann, H. F. and Friend, R. H., 1997. *An Improved Experimental Determination of External Photoluminescence Quantum Efficiency*. *Adv. Mater.*, **9**, 230-232.https://doi.org/10.1002/adma.19970090308.

Leyre, S., Coutino-Gonzalez, E., Joos, J. J., Ryckaert, J., Meuret, Y., Poelman, D., Smet, P. F., Durinck, G., Hofkens, J., Deconinck, G. and Hanselaer, P., 2014. *Absolute Determination of Photoluminescence Quantum Efficiency Using an Integrating Sphere Setup*. *Rev. Sci. Instrum.*, **85**, 123115.10.1063/1.4903852.

Bajar, B. T., Wang, E. S., Zhang, S., Lin, M. Z. and Chu, J., 2016. *A Guide to Fluorescent Protein Fret Pairs*. *Sensors*, **16**, 1488

Vogel, S. S., van der Meer, B. W. and Blank, P. S., 2014. *Estimating the Distance Separating Fluorescent Protein Fret Pairs*. *Methods*, **66**, 131-138.https://doi.org/10.1016/j.ymeth.2013.06.021.

Moreno, A. and Sipponen, M. H., 2020. *Lignin-Based Smart Materials: A Roadmap to Processing and Synthesis for Current and Future Applications*. *Mater. Horiz.*, **7**, 2237-2257.10.1039/D0MH00798F.

Sugiarto, S., Leow, Y., Tan, C. L., Wang, G. and Kai, D., 2022. *How Far Is Lignin from Being a Biomedical Material?* *Bioact. Mater.*, **8**, 71-94.https://doi.org/10.1016/j.bioactmat.2021.06.023.

Paul, S., Thakur, N. S., Chandna, S., Reddy, Y. N. and Bhaumik, J., 2021. *Development of a Light Activatable Lignin Nanosphere Based Spray Coating for Bioimaging and Antimicrobial Photodynamic Therapy*. *J. Mater. Chem. B*, **9**, 1592-1603.10.1039/D0TB02643C.

Wang, H., Liu, X., Yang, W., Mao, G., Meng, Z., Wu, Z. and Jiang, H.-L., 2022. *Surface-Clean Au25 Nanoclusters in Modulated Microenvironment Enabled by Metal–Organic Frameworks for Enhanced Catalysis*. *J. Am. Chem. Soc.*, DOI: 10.1021/jacs.2c09136.10.1021/jacs.2c09136.

Yu, Y., Luo, Z., Chevrier, D. M., Leong, D. T., Zhang, P., Jiang, D.-e. and Xie, J., 2014. *Identification of a Highly Luminescent Au22(Sg)18 Nanocluster*. *J. Am. Chem. Soc.*, **136**, 1246-1249.10.1021/ja411643u.

Nang An, V., Chi Nhan, H. T., Tap, T. D., Van, T. T. T., Van Viet, P. and Van Hieu, L., 2020. *Extraction of High Crystalline Nanocellulose from Biorenewable Sources of Vietnamese Agricultural Wastes*. *J. Polym. Environ.*, **28**, 1465-1474.10.1007/s10924-020-01695-x.

Tomczak, F., Sydenstricker, T. H. D. and Satyanarayana, K. G., 2007. *Studies on Lignocellulosic Fibers of Brazil. Part Ii: Morphology and Properties of Brazilian Coconut Fibers*. *Compos. Part A Appl. Sci. Manuf.*, **38**, 1710-1721.https://doi.org/10.1016/j.compositesa.2007.02.004.

Qian, H. and Jin, R., 2009. *Controlling Nanoparticles with Atomic Precision: The Case of Au144(Sch2ch2ph)60*. *Nano Lett.*, **9**, 4083-4087.10.1021/nl902300y.

Nimmala, P. R., Yoon, B., Whetten, R. L., Landman, U. and Dass, A., 2013. *Au67(Sr)35 Nanomolecules: Characteristic Size-Specific Optical, Electrochemical, Structural Properties and First-Principles Theoretical Analysis*. *The Journal of Physical Chemistry A*, **117**, 504-517.10.1021/jp311491v.

Yao, C., Chen, J., Li, M.-B., Liu, L., Yang, J. and Wu, Z., 2015. *Adding Two Active Silver Atoms on Au25 Nanoparticle*. *Nano Lett.*, **15**, 1281-1287.10.1021/nl504477t.

Wang, Z., Zhang, Q., Kuehner, D., Ivaska, A. and Niu, L., 2008. *Green Synthesis of 1–2 Nm Gold Nanoparticles Stabilized by Amine-Terminated Ionic Liquid and Their Electrocatalytic Activity in Oxygen Reduction*. *Green Chem.*, **10**, 907-909.10.1039/B806453A.

Dickerson, M. B., Sandhage, K. H. and Naik, R. R., 2008. *Protein- and Peptide-Directed Syntheses of Inorganic Materials*. *Chem. Rev.*, **108**, 4935-4978.10.1021/cr8002328.

Krauss, E., Kullock, R., Wu, X., Geisler, P., Lundt, N., Kamp, M. and Hecht, B., 2018. *Controlled Growth of High-Aspect-Ratio Single-Crystalline Gold Platelets*. *Cryst. Growth Des.*, **18**, 1297-1302.10.1021/acs.cgd.7b00849.

Oh, E., Huston, A. L., Shabaev, A., Efros, A., Currie, M., Susumu, K., Bussmann, K., Goswami, R., Fatemi, F. K. and Medintz, I. L., 2016. *Energy Transfer Sensitization of Luminescent Gold Nanoclusters: More Than Just the Classical Förster Mechanism*. *Sci. Rep.*, **6**, 35538.10.1038/srep35538.

Supplementary data for

Fluorescence Switching of Natural Fibers with in-situ Formation of Gold Nanoclusters

Yong Yu,[1]* Ying Chuan Tan,[2] Gorelik Sergey,[3] Yihao Leow,[1] Hui Ru Tan,[1] Chi-Lik Ken Lee [4], Qiang Zhu[1,2,4], Enyi Ye,[1,2,4] Le Yang,[1,5] Dan Kai *[1,2,4]

[1] Institute of Materials Research and Engineering (IMRE), A*STAR, 2 Fusionopolis Way, #08-03, Innovis, 138634, Singapore

[2] Institute of Sustainability for Chemicals, Energy and Environment (ISCE2), A*STAR, 2 Fusionopolis Way, Innovis, #08-03, 138634, Singapore

[3] Singapore Institute of Food and Biotechnology Innovation (SIFBI), A*STAR, 31 Biopolis Way, #01-02, Nanos, 138669, Singapore

[4] Division of Chemistry and Biological Chemistry, School of Physical and Mathematical Sciences, Nanyang Technological University, 21 Nanyang Link, Singapore 637371, Singapore

[5]Department of Materials Science and Engineering, College of Design and Engineering, 9 Engineering Drive 1, National University of Singapore, 117575, Singapore

Email: yuy@imre.a-star.edu.sg; kaid@imre.a-star.edu.sg

Supporting figures and tables

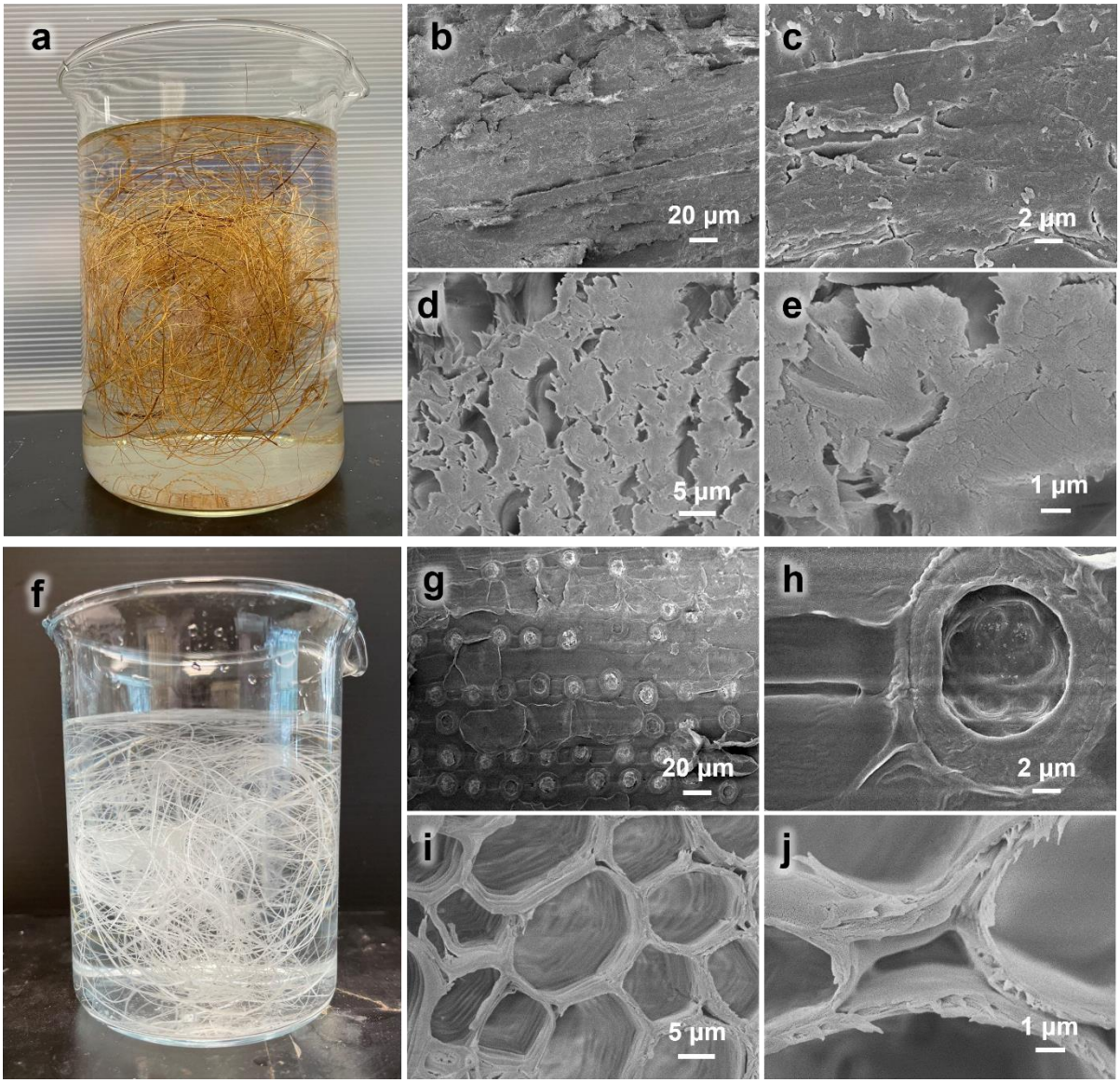

Fig. S1. (a) Photographic image of raw coir soaked in water, and SEM images of its (b, c) surface and (d, e) cross-section features. (f) Photographic image of delignified coir soaked in water, and SEM images of its (g, h) surface and (e, j) cross-section features.

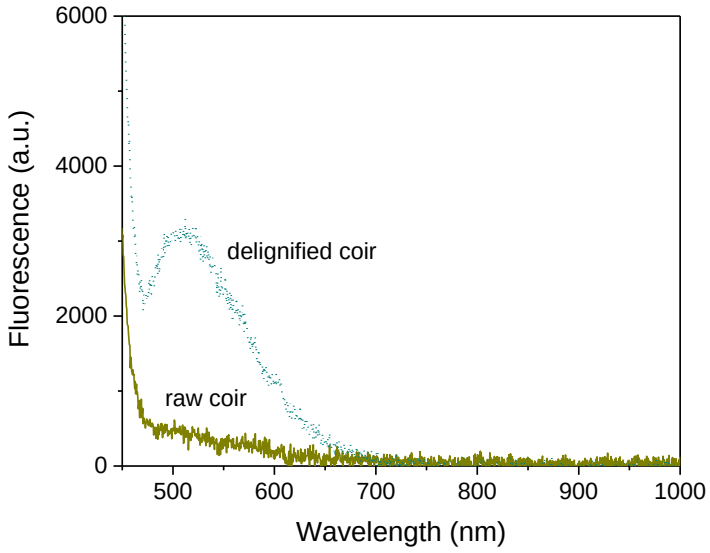

559

560 **Fig. S2**. Fluorescence spectrum of the raw coir fiber prior to delignification. The dotted line is
561 the fluorescence spectrum of the delignified coir included for comparison purpose only.

562

563 **Table S1**. Thermogravimetric results of the delignified coir (Fig. 1c, item ***1***) and coir@AuNC
564 (Fig. 1c, item ***2***) (atmosphere: N_2).

Sample	**Transition temperature range (°C)**	**Transition peak (°C)**	**Weight loss (%)**	**Residue (%)**
Delignified coir	30-107	61	5	
	205-310	274	26	
	310-420	357	44	24
coir@AuNC	25-103	58	6	
	195-425	343	68	
	450-800	566	24	2

565

566

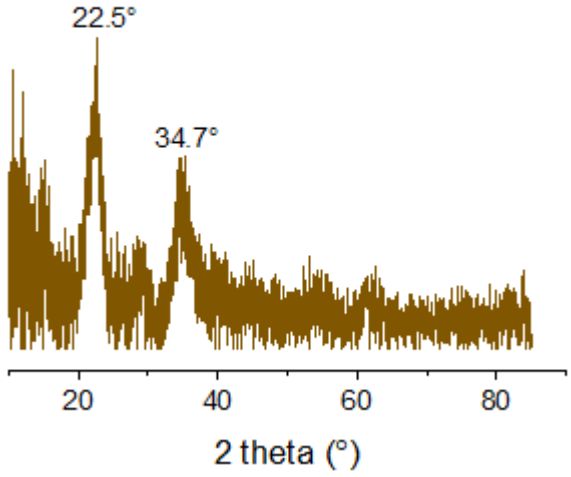

Fig. S3. XRD spectrum of the raw coir fiber without delignification.

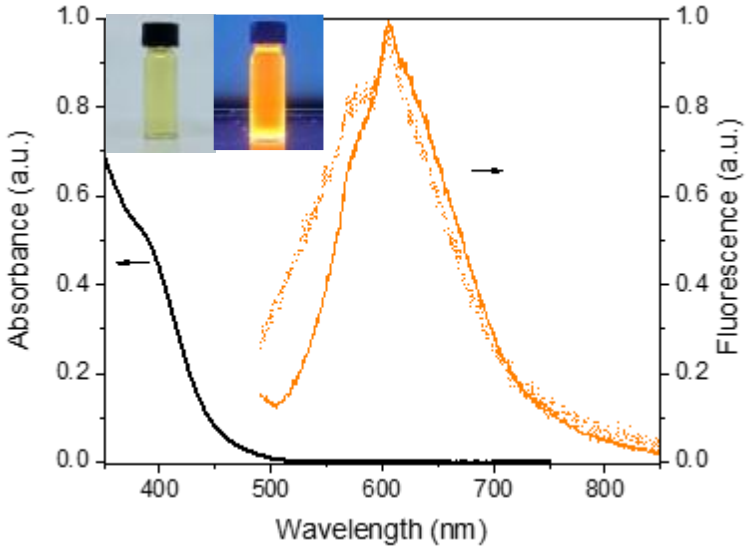

Fig. S4. UV-vis absorption spectrum (black) and fluorescence spectrum (orange, λ_{ex} = 405 nm) of the supernatant separated from the synthesis mixture. The dot line represents the fluorescence spectrum of coir@AuNC. The difference in both spectra suggests the in situ formed AuNC strongly interact with the delignified coir and is different from that formed in

the supernatant. (Inset) Digital photos of the supernatant under daylight and UV light, respectively.

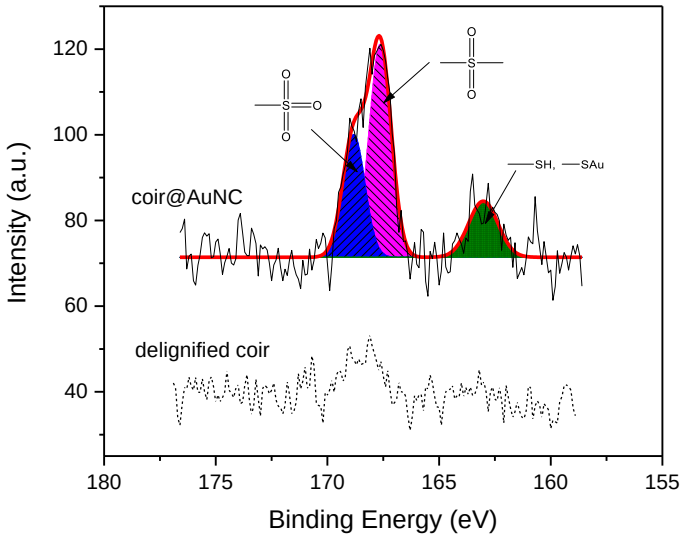

Fig. S5. XPS high resolution S2p spectra of delignified coir and coir@AuNC.

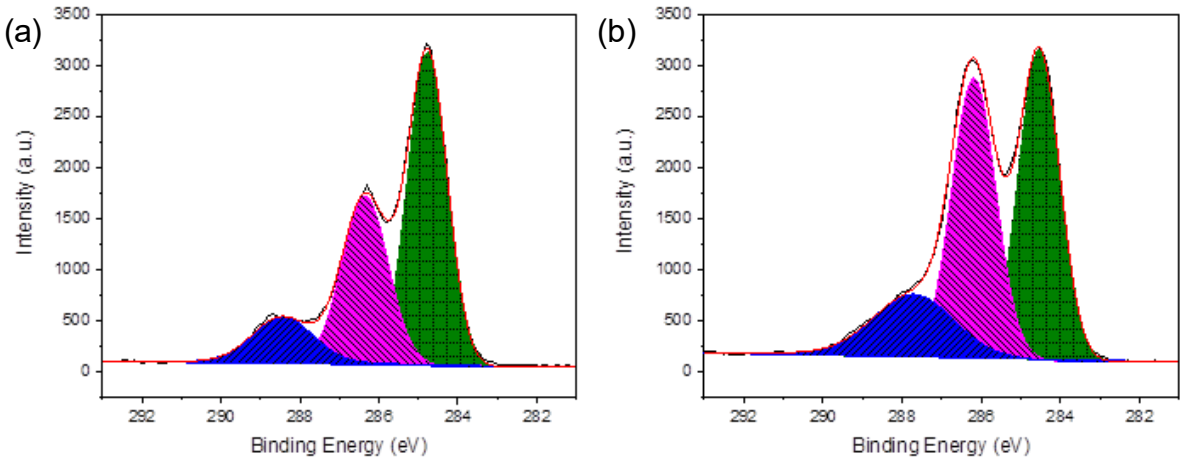

(c)

Binding energy (eV)	Assignment	Relative abundance (vs C-C and C-H)	
		Delignified coir	coir@AuNC
284.8	C-C, C-H	1	1
286.3	C-OH, C-S,* C-N*	0.6	0.9
288.4	O–C–O, C-N,* O-C=O*	0.2	0.4

583 **Fig. S6**. XPS high resolution C1s spectra of (a) delignified coir and (b) coir@AuNC. (c)
584 Assignment of possible components in the deconvoluted spectra. The stars indicate the
585 components contributed by GSH.

586 **Table S2**. Lifetimes of emitting species in delignified coir and coir@AuNC by exponential
587 fitting of the experimental data in Fig. 3

	τ_1 [ns] (relative amplitude)	τ_2[ns] (relative amplitude)	$\tau_{average}$ [ns]	χ^2	Note
Delignified coir	0.82 (62%)	3.20 (38%)	2.50	1.00	
coir@AuNC	0.76 (64%)	3.05 (36%)	2.34	1.00	430 nm longpass filter
	3.29 (1%)	514.21 (99%)	514.19	0.91	600 nm longpass filter

588

589 **Table S3**. Refractive indices of selected solvents.

Solvent	Refractive index *(n)*	Remarks
Acetonitrile	1.344	Polar aprotic
Acetone	1.359	Polar aprotic
Methanol	1.326	Polar protic
Ethanol	1.361	Polar protic
DMSO	1.479	Polar aprotic
2-Propanol	1.378	Polar protic

THF	1.407	Polar aprotic
Water	1.333	Polar protic

590

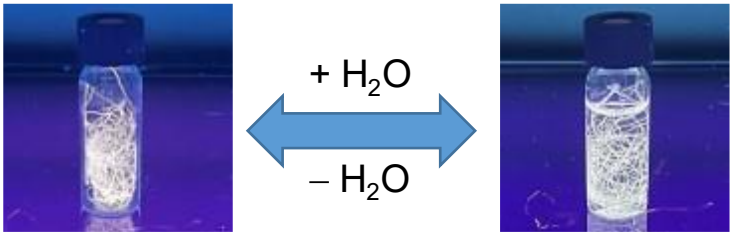

591

592 **Fig. S7**. Reversable emission color change of the coir@AuNC in dry state and water.